PHYSICAL REVIEW B VOLUME 23, NUMBER 12 15 JUNE 1981

Investigation of the vibronic properties of Cu_3VS_4, Cu_3NbS_4, and Cu_3TaS_4 compounds

D. Petritis and G. Martinez

Laboratoire de Physique des Solides, Associé au Centre National de la Recherche Scientifique, Université Pierre et Marie Curie, 4 place Jussieu, 75230 Paris Cédex 05, France

C. Levy-Clement and O. Gorochov

Laboratoire de Physique des Solides, Centre National de la Recherche Scientifique, 1 place Aristide Briand, 92190 Meudon, France

(Received 26 February 1980)

Infrared-reflectivity results on Cu_3VS_4 and Raman scattering data as a function of temperature and hydrostatic pressure for Cu_3MS_4 (with M = V, Nb, Ta) are reported. The group-theoretical analysis on the sulvanite compounds is performed allowing the assignment of optically active modes. The mode anharmonicity is determined using standard methods, and experimental evidence of an anharmonic resonance phenomenon is explained by a simple model. Most of the experimental results are discussed in connection with the physical properties of the compounds.

I. INTRODUCTION

The members of the isostructural family Cu_3MS_4 (M = V, Nb, Ta) have some special structural features common to the majority of solid electrolytes. In addition to a normal electronic conduction (Cu_3VS_4 is a p-type semiconductor), Cu_3VS_4 has a weak ionic conductivity[1] at room temperature, due to the migration of Cu^+ ions.

This ionic motion gives rise to modes not expected to be seen in Raman scattering experiments due to their low frequency. However, indirect effects of coupling between these modes and the normal modes, could in principle be allowed. This is expected to be revealed by the value and variation of the anharmonicity of normal modes.

This paper reports the evaluation of the anharmonicity obtained from measurements of modes as a function of temperature and pressure. This study is performed, after the assignment and measurements of all active modes, from infrared-reflectivity and Raman scattering experiments, coupled to a group-theoretical analysis of the structure. Only intrinsic results, obtained with a large number of samples both in crystalline and powder form, are reported.

II. GENERAL PROPERTIES OF THE COMPOUNDS

A. Structural properties

The Cu_3MS_4 (M = V, Nb, Ta) compounds crystallize in the simple cubic system[2] with one molecular unit (eight atoms) per unit cell. They exhibit the T_d group symmetry and Fig. 1 sketches the arrangement of the atoms within the unit cell. Worth noting is the large number of empty sites allowed by symmetry along the cube edges and on the cube corners. These empty sites form a three-dimensional network of empty crystallographic channels along the ⟨100⟩ direction. The structural parameters of the three compounds are shown in Table I. The structure described above was refined on a large number of experimental points for Cu_3VS_4 (Ref. 3) and the electron-density distribution was calculated for that compound. It turns out that the electron-density corresponding to the sulfur, instead of being spherically symmetric with its center along ⟨111⟩ directions, is distorted in a triangular asteroid fashion with an excess density following the $\langle 11\bar{2}\rangle$ direction on the (111) plane. This distortion is interpreted by Trojer[3] as a strongly anharmonic motion of the sulfur atom or a static distortion. The x-ray diffraction pattern for the copper atoms was also found abnormal with a pronounced smearing and a very small intensity. A new refinement of the structure performed by Collin and Le Nagard[4] suggested that the Cu atom occupies one of the four equivalent positions defined by a slight displacement of 0.14 Å following the ⟨100⟩ directions in the cubic face. From the published data, it is difficult to know if these distortions are ortho-

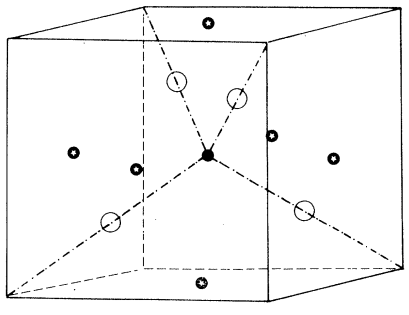

FIG. 1. Unit cell of Cu_3MS_4.

TABLE I. Structural parameters of Cu_3MS_4.

Cu_3MS_4	Lattice parameter a (Å)	Metal-sulfur distance (Å)	Off-centering of the copper atom (Å)
Cu_3VS_4	5.391 ±0.002	2.186	0.14
Cu_3NbS_4	5.500 ±0.002	2.24	
Cu_3TaS_4	5.525 ±0.02	2.24	

gonal to each other or equivalent descriptions of the same effect.

Some further structural considerations are possible: The Cu_3MS_4 belong to the T_d group symmetry; then the mechanical representation with eight atoms per cell decomposes as

$$\Gamma_{mec} = A_1 \oplus E \oplus 2F_1 \oplus 5F_2 .$$

Among these modes, four F_2 modes are both Raman and infrared active, A_1 and E modes are only Raman active, and the acoustic F_2 modes and the two F_1 modes are inactive in our experiments.

B. Preparation of the samples

The synthesis of the isostructural phases of Cu_3MS_4 is made by a chemical reaction between the copper sulfide (Cu_2S) and the metal sulfide (M_2S_3). The metallic elements (99.9% pure) are reducted by hydrogen at temperatures varying between 500 °C and 900 °C, the hydrides eventually synthesized being decomposed under vaccum at high temperature. The sulfur is purified by distillation to 99.999 9% pure and copper sulfide is made by direct reaction. Then the Cu_3MS_4 compounds are obtained in a second step by mixing the binary sulfides at 750–800 °C. The resulting phases are controlled by x-ray diffraction.

Monocrystals of the compounds are obtained by vapor transport with chemical agents like chlorine (60 mm Hg at 300 K). The temperatures of the hot point are 720 °C for Cu_3VS_4 and 800 °C for Cu_3NbS_4 and Cu_3TaS_4, crystals being collected at a temperature of 40 °C below these.

The vapor transport takes about two weeks to produce rather large slabs of Cu_3VS_4 ($2 \times 3 \times 5$ mm^3) but only small cubes of Cu_3Nb_4 and Cu_3TaS_4 of about 1-mm edge.

C. Electronic gap

An infrared-absorption experiment in the energy range of electronic transitions has been performed on thin polished Cu_3VS_4 samples. Figure 2 shows the experimental results at both room and liquid-nitrogen temperatures. No simple standard law

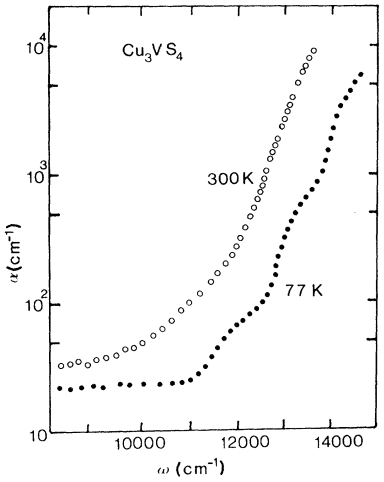

FIG. 2. Absorption coefficient of Cu_3VS_4.

reproduces the variation of the absorption coefficient at room temperature. At lower temperatures the absorption coefficient exhibits structures, a complete study of which would necessitate measurements at liquid-helium temperatures. These structures are probably connected with multiple transitions between the d bands of the copper and those of the transition metal. For Cu_3VS_4 the gap lies approximately at 1.3 eV.

The two other compounds Cu_3NbS_4 and Cu_3TaS_4 are red and yellow-green, respectively, and this is the only information we have about their gap. No absorption measurements are possible for these two compounds because of their small sizes; thus, any polishing manipulation of them failed. No other information about the electronic properties of these materials is known. No band-structure data are available, and in view of our main interest in the study of their vibronic properties, we did not perform the study of any galvanomagnetic properties.

III. EXPERIMENTAL PROCEDURE

For the infrared-reflectivity and near-infrared absorption measurements on Cu_3VS_4, the samples are polished. For reflectivity measurements, the polishing procedure used fine diamond powder suspension in oil with 0.5-μm grains. For transmission measurements, best results were obtained when the polishing was performed parallel to a natural growth face. In this case only one face had to be polished. With this method we prepared samples with a thickness down to 8 μm and a face parallelism good enough to obtain interferences. For Raman scattering we used either samples with natural faces or samples cleaved along crystallographic directions. Raman scattering on

polished surfaces was performed only for test measurements. All samples, except the cleaved ones, were abundantly washed with pure alcohol before the measurements.

The infrared-reflectivity spectrum of Cu_3VS_4 is obtained with a single grating far-infrared Coderg monochromator aligned with a Golay detector and an infrared globar source. The infrared-absorption spectrum of Cu_3VS_4 is obtained with a double grating Coderg monochrometer followed by a photomultiplier working at the continuous regime as the detector.

The various Raman spectra were obtained with a double or triple grating Coderg monochromator: The instrumental resolution was usually of 1 cm^{-1} but never exceeded 4 cm^{-1} for the weaker structures. Furthermore, in order to have physically meaningful and comparable results, the experimental spectra were deconvoluted by the response function of the monochromator. As an exciting source, an Ar^+ or Kr^+ laser of coherent radiation was used. The laser power on the sample never exceeded 50 mW and was usually of the order of 10 mW in order to avoid excess heating and to have a reliable measure of temperature. The detection was performed by a cooled RCA photomultiplier working with a photon-counting chain.

The spectra as a function of temperature were obtained using an air liquide helium cryostat or a small liquid-nitrogen cryostat. In both of them, the temperature was electronically regulated to ±2 K during the measurements.

For pressure-dependent measurements, some of the high-pressure techniques developed during the last years have been used. In the high-pressure range, the hydrostatic pressure up to 100 kbars is obtained with the gasketed diamond anvil high-pressure cell.[5] A small sample is introduced in a hole of about 80-μm height and 200 μm in diameter opened in the gasket. A small ruby crystal is also introduced as a pressure gauge together with a drop of 4:1 methanol-ethanol mixture as pressure-transmitting medium. In the low-pressure range a conventional maraging steel high-pressure cell is used. Four sapphire windows on each side of the cell allow optical experiments;

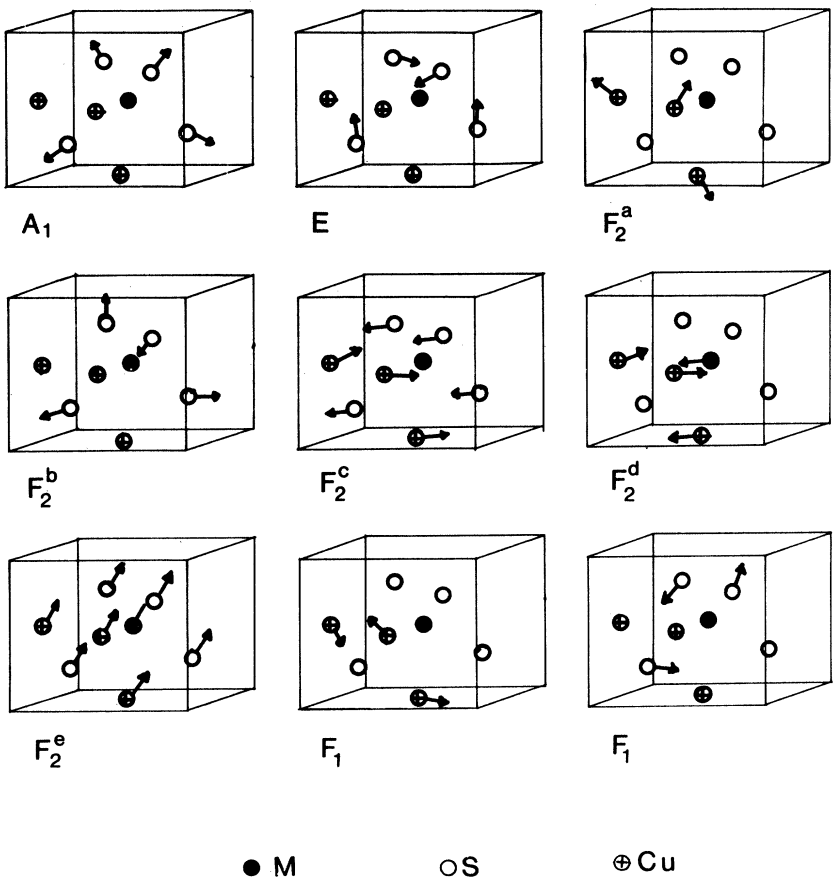

FIG. 3. "Eigenmotions" of the atoms for the various modes of the sulvanite structure.

pressure is transmitted by a stainless-steel tube of 0.3-mm inner and 1.6-mm outer diameter. The pressurizing medium is a highly purified helium gas. The whole high-pressure cell can merge in a special cryostat allowing experiments at 300 and 77 K in varying pressures between 0–10 kbar. Inside the high-pressure cell there is enough room for mounting ordinary samples of about 0.5 cm^3.

IV. MODE ASSIGNMENT

For each vibrational mode, eigenvectors of the dynamical matrix can be computed but this is an extremely difficult task and presumes the complete solution of the dynamical problem. On the other hand, what we need is not the eigenvectors of the dynamical matrix with their absolute phase factors but only the way the atoms move inside the unit cell for a given mode-A special computer program[6] allows the construction of symmetry coordinates. The eigenvectors are linear combinations of the symmetry coordinates and have to fulfill the mutual orthonormality and the immobility of the center-of-mass (for the optical modes) conditions. Figure 3 sketches the way every atom of the unit cell moves for a given mode.

Once the motions are computed, the problem stems from the fact that the experimentally observed frequencies have to be attributed to the corresponding "eigenmotions." Raman scattering for various polarizations of the incident and scattered beams in the backscattering geometry allows the identification of A_1, E, and F_2 modes, according to the standard selection rules of the T_d group in that configuration. For a complete assignment of the F_2^e $(e=a,b,c,d)$ modes we need some additional results.

An infrared-reflectivity experiment is performed on Cu_3VS_4; Fig. 4 shows the results obtained at 300 K. Three of the four infrared-active F_2 modes are observed; the fourth one which lies at the lowest frequency is not seen in the range of energy scanned by our experimental setup. Standard Kramers-Kronig analysis[7] of the reflectivity data leads to the determination of the complex dielectric function $\epsilon(\omega)$. The TO and LO frequencies of the active polar modes and their oscillator strengths are also determined from the analysis of the experimental data. Qualitatively, the TO-LO splitting is a measure of the ionicity of the sample for the corresponding mode; the oscillator strength is related to the electric dipole moment of the mode. Table II summarizies the reflectivity results and shows an ionicity and an oscillator strength for the high-frequency F_2 mode 1 order of magnitude higher than for the other modes. The comparison of these results with

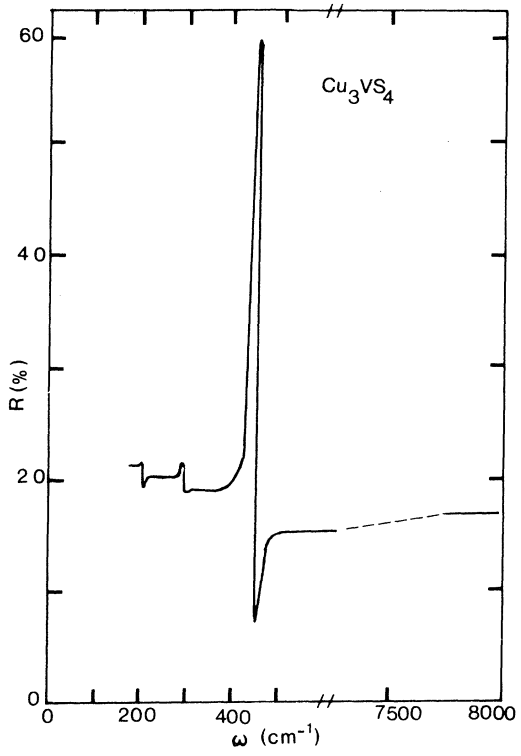

FIG. 4. Reflectivity spectrum of Cu_3VS_4 at 300 K.

those reported in the literature[8] for the two other substitutional compounds and the calculation of the electric dipole moment for each polar mode allows the assignment of the observed frequencies to the corresponding eigenmotions. The complete assignment is shown in Table III.

V. RAMAN SCATTERING EXPERIMENTS

All the infrared-active modes are also Raman active for the Cu_3MS_4 materials. Furthermore, Raman scattering is a much more versatile technique, as far as temperature and high-pressure experiments are concerned, because no absolute intensity measurements are necessary to detect the main dynamical behavior of the system.

TABLE II. Results of the frequency and oscillator-strength determinations for the different F_2 modes of Cu_3VS_4 at 300 K.

	Cu_3VS_4 (300 K)		
Mode	TO (cm^{-1})	LO (cm^{-1})	ρ_i (cm^{-2})
F_2^b	202.3	204.1	1.7×10^4
F_2^c	286.3	287.5	4.1×10^4
F_2^d	440.3	450.1	2.3×10^5

TABLE III. Frequency (cm^{-1}) and assignment of vibrational modes of Cu_3MS_4 compounds.

Mode	Cu_3VS_4	Cu_3NbS_4	Cu_3TaS_4
A_1	375.6	404	414.3
E	301.2	265.2	265.5
F_2^a	147.2	122.1	114.3
F_2^b	201.4	196.4	178.8
F_2^c	286.4	245.5	
F_2^d	439.6 448.4	440.0	420.4

Therefore, the subsequent study turned into a detailed Raman spectroscopic analysis.

Figure 5 shows the complete Raman spectra obtained for the three materials in a backscattering geometry and the $X(ZZ)\bar{X}$ polarization at 300 K. For the $X(YZ)\bar{X}$ polarization, the A_1-mode intensity decreases by 2 orders of magnitude but the expected F_2-mode enhancement is rather poor. The intensity scale in arbitrary units gives an idea of the relative intensities.

A systematic study of the phonon energies and lifetimes was first performed as a function of the temperature. Table IV summarizes the characteristics of the straight lines of the form $\omega(T) = \omega_0 + aT$ and $2\Gamma(T) = 2\Gamma_0 + bT$ fitted on the experimental results for the three materials. Some slightly negative values for $2\Gamma_0$ that appear in that table have, of course, no physical significance; they are the result of a numerical extrapolation to $T = 0$ K for a straight line fitted at high temperature ($T > 77$ K) only. Some special features in that table are worth noting.

(i) For Cu_3NbS_4 and Cu_3TaS_4 there appears in the table a peak labeled A' that is not predicted by symmetry.

(ii) No F_2^c mode appears for Cu_3TaS_4 probably because it is extremely weak. In fact F_2^c is the weakest mode for the other two compounds.

(iii) The TO-LO splitting is obtained for only the F_2^d mode of Cu_3VS_4. The only plausible explanation is that the ionicity for the other two compounds is significantly lower than that of Cu_3VS_4.

(iv) The frequency of all the modes except the A_1 mode decreases when the atomic number of M atom increases.

(v) All compounds exhibit nearly the same behavior: E and F_2 modes vary rapidly with temperature in contrast to the soft variations of A_1 modes.

(vi) The full width at half maximum (FWHM) of the A_1 mode of Cu_3VS_4 is, at all temperatures, 2 to 3 times as large as the FWHM of the same mode for the other compounds.

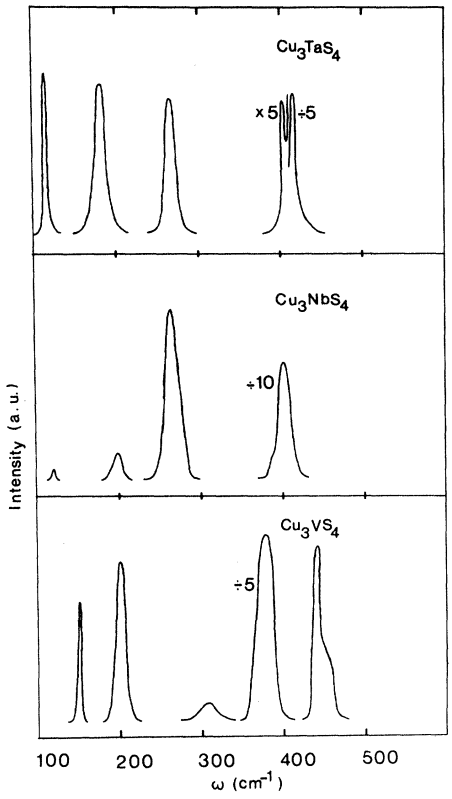

FIG. 5. Raman spectra for the Cu_3MS_4 compounds in the $X(ZZ)\bar{X}$ configuration.

Next, the pressure dependence of the phonon frequencies was examined. Phonon-lifetime measurements become much more difficult and are measured only for the modes with a large Raman cross section. The Raman spectra in pressure experiments are extracted with a point-by-point technique where photon counts are stored for sufficient time in a 1-cm^{-1}-width channel.

Two kinds of pressure experiments are performed. Table V summarizes the results obtained in the diamond anvil high-pressure cell. The very weak Raman signal and the high level of the background noise prohibits the detection of any reliable peak for the weakest modes.

Cu_3NbS_4 and Cu_3TaS_4, under pressure, exhibit a phase transition at about 25 and 35 kbar, respectively. The approach of the phase transition is characterized by a rapid decrease of the Raman activity. The samples are transformed into a black metallic-looking powder after the phase transition with no detectable Raman activity between 10 and 600 cm^{-1}. The signal coming from Cu_3VS_4 decreases considerably approaching 90 kbars suggesting a probable phase transition in

TABLE IV. Parameters for the variations of the frequency $\omega = \omega_0 + aT$ and the width $2\Gamma = 2\Gamma_0 + bT$ of the Cu_2MS_4 modes as a function of temperature. Both quantities have been assumed to vary linearly above 77 K.

Mode	ω_0 (cm^{-1})	a ($10^{-2}\,cm^{-1}deg^{-1}$)	$2\Gamma_0$ (cm^{-1})	b ($10^{-2}\,cm^{-1}deg^{-1}$)	ω_0 (cm^{-1})	a ($10^{-2}\,cm^{-1}deg^{-1}$)	$2\Gamma_0$ (cm^{-1})	b ($10^{-2}\,cm^{-1}deg^{-1}$)
		Cu_3VS_4				Cu_3NbS_4		
A'					403.9	−0.9	−0.1	0.7
A_1	377.6	−0.7	1.7	1.4	407.9	−1.4	−0.1	0.7
E	308.4	−2.5	0.9	1.5	269.8	−1.5	−0.9	2.6
F_2^a	156.8	−2.6	−0.3	1.1	130	−2.6	−1.6	2.3
F_2^b	209.6	−2.2	0.3	1.3	200.5	−1.4	−0.1	2.3
F_2^c	293.4	−2.2	1.7	1.8	250.9	−1.8	−1.0	2.6
F_2^d	445.5	−1.7	0	1.0				
	455.7	−1.5	−0.2	1.2	444.8	−1.6	0.0	0.8
		Cu_3TaS_4						
A'	406.2	−1.0	0.2	0.7				
A_1	416.6	−1.0	0.0	1.0				
E	271.8	−1.8	−0.8	1.5				
F_2^a	121.2	−2.2	−1.4	1.4				
F_2^b	183.6	−1.5	−0.5	2.3				
F_2^c								
F_2^d								
	424.0	−1.2	0.0	0.3				

that region.

With the metallic high-pressure cell, the same kind of experiment was performed at 300 and 77 K but in a pressure range restricted to 10 kbar. Table VI summarizes the experimental results.

A general remark can be made for the experimentally observed behavior: The E- and F_2-mode frequencies for all three compounds vary much more rapidly than the A_1-mode frequencies under pressure. A small tendency to the saturation of the variation of $d\omega/dP$ is observed for Cu_3NbS_4 and Cu_3TaS_4 near the phase transition; this fact is reflected on the slightly lower values of the determined slopes $c = d\omega/dP$ in the high-pressure regime than in the low-pressure one. No remarkable changes of the FWHM are detected within the experimental accuracy except for the A_1 mode of Cu_3VS_4, as will be discussed in Sec. VIII.

TABLE V. Variation of the frequency ω of the Cu_3MS_4 modes as a function of pressure up to 80 kbar, at 300 K. The results have been fitted to a linear law of the form $\omega = \omega_0 + cP$.

Mode	ω_0 (cm^{-1})	C ($cm^{-1}\,kbar^{-1}$)	ω_0 (cm^{-1})	C ($cm^{-1}\,kbar^{-1}$)	ω_0 (cm^{-1})	C ($cm^{-1}\,kbar^{-1}$)
	Cu_3VS_4		Cu_3NbS_4		Cu_3TaS_4	
A'			400.5	$(2\pm1)\times10^{-2}$	403.3	$(0\pm3)\times10^{-3}$
A_1	375.8	$(-7\pm1)\times10^{-2}$	403.7	$(0\pm3)\times10^{-3}$	413.3	$(0\pm3)\times10^{-3}$
E	302.4	0.7	265.6	0.6	267	0.6
F_2^a	148.4	0.6			114.4	0.3
F_2^b	204.3	0.6			179.6	0.6
F_2^c						
F_2^d	440.9	0.2				
	449.6	0.1				

VI. MODE ANHARMONICITY

As is known from anharmonic theory,[9] free phonons are renormalized in the presence of anharmonic interactions and within the quasiharmonic approximation; their frequency ω_h acquires a complex self-energy part in the form

$$\omega \simeq \omega_h + \Sigma = \omega_h + \Delta + i\Gamma \,, \tag{1}$$

where Δ is the frequency shift relative to the harmonic phonon frequency ω_h, and 2Γ is the FWHM (inverse of the lifetime of the anharmonic "phonon"). Explicit forms of the self-energy Σ have been reported[10] for low-order perturbation and anharmonicity. Final results are summarized here:

$$\Sigma_4(z) = \frac{12}{\hbar} \sum_{\vec{q}_1, j_1} V_4(-\vec{q}j;\vec{q}j';\vec{q}_1 j_1;-\vec{q}_1 j_1)(2n_1+1) \,,$$

$$\Sigma_6(z) = -\frac{18}{\hbar^2} \sum_{\vec{q}_1, j_1; \vec{q}_2, j_2} |V_3(\vec{q}j, \vec{q}_1 j_1; \vec{q}_2 j_2)|^2 \tag{2}$$

$$\times \left[(n_1+n_2+1)\left(\frac{1}{z+\omega_1+\omega_2} - \frac{1}{z-\omega_1-\omega_2}\right) + (n_1-n_2)\left(\frac{1}{z-\omega_1+\omega_2} + \frac{1}{z+\omega_1-\omega_2}\right)\right],$$

where $\omega_i = \omega(\vec{q}_i j_i)$, $\beta = 1/kT$, and $n_i = [\exp(\beta\hbar\omega_i - 1)]^{-1}$. V_3 and V_4 are the three- and four-phonon interaction potentials, respectively. The summations extend to the whole Brillouin zone and, unless the density of states and the anharmonic interactions are known for the whole Brillouin zone, the formulas have no computational interest. For that reason, in most cases a phenomenological treatment of the anharmonicity is performed, directly connected with the experimental results.

A pressure experiment acts on the volume of the crystal and consequently on the photon energies, because for a real crystal they depend on the volume. Within the Grüneisen approximation, this dependence is scaled in the following manner:

$$\frac{d\omega_i}{\omega_i} = -\gamma_i \frac{dV}{V} \Rightarrow \frac{d(\ln\omega_i)}{dP} = \gamma_i K \,, \tag{3}$$

where γ_i is the Grüneisen parameter of the ith mode and K the isothermal compressibility. Once the isothermal compressibility is known, the Grüneisen parameter is directly determined from the experimental results by means of Eq. (3). Zallen and Slade[11] have proposed a model valid for molecular crystals. In that mode, γ_i has an high constant value for the external (soft) modes and its value decreases as $\gamma_i \sim \omega_i^{-2}$ for the internal (hard) modes. Figure 6 illustrates the calculated results for the Cu_3MS_4 samples. We looked for any possible "molecular" behavior of our samples in the form of an MS_4^{3-} molecule with weakly bonded Cu^+ ions. But this model is clearly not realistic in fact, the E modes have a high value, although they are internal modes of MS_4^{3-}, and F_2^4 a very low γ value whereas it should be an external mode for this molecule; the A_1 modes have a completely singular behavior within this model. Therefore the Cu_3MS_4 have a more compact bonding picture and this fact must be taken into account in lattice-dynamical considerations.

A temperature experiment has a more complicated effect on the observed frequencies. A real (i.e., anharmonic) crystal changes its volume under temperature variations as a consequence of thermal expansion. The phonon population is also temperature dependent as a consequence of the Bose-Einstein statistics, i.e., the Green's functions in the renormalization equation are temperature dependent. So the temperature dependence of the phonon frequency is conventionally split into two terms as follows:

$$\frac{d\omega_i}{dT} = \frac{\partial\omega_i}{\partial T} - \frac{\alpha}{K}\frac{\partial\omega_i}{\partial P} \,, \tag{4}$$

where α is the isobaric thermal expansivity. The slopes $d\omega_i/dT$ and $\partial\omega_i/\partial P$ are experimentally determined. The intrinsic (population) effect $\partial\omega_i/\partial T$ of the temperature can be determined if the α/K ratio is measured.

X-ray-diffraction experiments on Cu_3VS_4 gave a value for $\alpha \simeq 1\times10^{-6}$ deg^{-1}. Isothermal compressibility K has been also estimated for this crystal by a photographic method in the diamond anvil cell to be $K \simeq 1\times10^{-5}$ bar^{-1}. This method consists of taking pictures under the microscope for various pressures and is very approximate. In any way, even if the determined value of α/K is not precise, it introduces only a systematic error. The same α/K ratio is used at both temperatures 300 and 77 K for all three compounds for lack of other experimental information. We have already reported[12] results on Cu_3VS_4. Here complete results for all three compounds are shown and Table VII summarizes the main features.

TABLE VI. Variation of the frequency ω of the Cu_3MS_4 modes as a function of the pressure up to 10 kbar at 300 and 77 K. The results are fitted in the same way that those reported in Table V.

	Cu_3VS_4				Cu_3NbS_4				Cu_3TaS_4			
	300 K		77 K		300 K		77 K		300 K		77 K	
Mode	ω_0 (cm^{-1})	c (cm^{-1} kbar^{-1})	ω_0 (cm^{-1})	c (cm^{-1} kbar^{-1})	ω_0 (cm^{-1})	c (cm^{-1} kbar^{-1})	ω_0 (cm^{-1})	c (cm^{-1} kbar^{-1})	ω_0 (cm^{-1})	c (cm^{-1} kbar^{-1})	ω_0 (cm^{-1})	c (cm^{-1} kbar^{-1})
A'					401.3	$0 \pm 1 \times 10^{-2}$	403.4	$0 \pm 1 \times 10^{-2}$	403.2	$0 \pm 1 \times 10^{-2}$	405.0	$0 \pm 1 \times 10^{-2}$
A_1	375.9	$0 \pm 1 \times 10^{-2}$	376.9	$0 \pm 1 \times 10^{-2}$	403.7	$6 \pm 1 \times 10^{-2}$	407.0	-0.1	414.1	$0 \pm 1 \times 10^{-2}$	416.0	$0 \pm 1 \times 10^{-2}$
E	302.2	0.7	306.0	0.8	265.3	0.7	269.3	0.7	266.0	0.7	269.9	0.7
F_2^a	148.8	0.6	154.4	0.6	121.4	0.8	127.8	0.4	11.5	0.4	119.0	0.3
F_2^b	204.0	0.6	208.2	0.7	197.2	0.6	201.0	0.5	178.4	0.8	182.0	0.7
F_2^c					244.7	1.2	250.0	0.7				
F_2^d	441.1	0.2	444.6	0.2	439.8	0.2	443.5	$2 \pm 1 \times 10^{-2}$	419.6	0.1	422.5	$2 \pm 1 \times 10^{-2}$
	450.0	0.1	452.4	0.2								

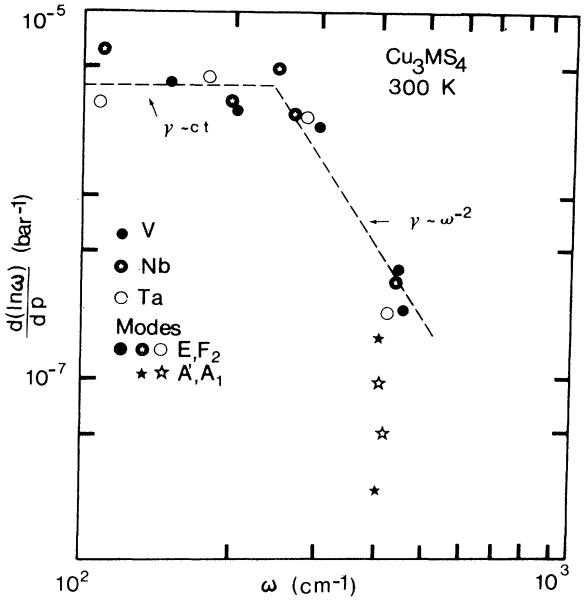

FIG. 6. Grüneisen parameters of Cu_3MS_4.

A general remark can be made on the sign of the intrinsic anharmonicity: It is always negative for our samples. An inspection of the anharmonic terms [Eq. (2)] shows that third-order terms have either a positive or a negative contribution in contrast to fourth-order terms that have always a positive contribution. Geometrical and colloquialism arguments show that V_4 and $|V_3|^2$ should be of the same order of magnitude, in the first approximation, which means that third- and fourth-order anharmonicity should contribute similarly. In reality, this is not true because Σ_4 is roughly a constant in contrast to Σ_6 which is modulated by a frequency-dependent function.

The real part of this frequency function exhibits a pulselike shape, characteristic of the Kramers-Kronig inversion of a Lorentzian, only in the neighborhood of $\omega = \omega_1 \pm \omega_2$. Away from the resonance region this function has a small, roughly constant value.

So, even away from a resonance this function can have a small non-negligible value. It is also worth noting that $\Sigma_4(z)$ is independent of z in a first approximation. z is a probing frequency generally taken equal to the phonon frequency. This means that for a given temperature fourth-order anharmonic contributions are roughly the same for all phonons in the crystal. This is also true for $\Sigma_3(z)$ away from the resonance regions.

An overall negative sign of $\partial\omega/\partial T$ (as shown in Table VII) can be interpreted as a dominance of third-order anharmonicity over the fourth-order one. The similar values of $\partial\omega/\partial T$ obtained for

TABLE VII. Total anharmonicity parameters deduced from Eq. (4) for the Cu_3MS_4 compounds.

Mode	Cu_3VS_4 $\partial\omega/\partial T$ (10^{-2} cm^{-1}deg^{-1}) 300 K	77 K	Cu_3NbS_4 $\partial\omega/\partial T$ (10^{-2} cm^{-1}deg^{-1}) 300 K	77 K	Cu_3TaS_4 $\partial\omega/\partial T$ (10^{-2} cm^{-1}deg^{-1}) 300 K	77 K
A'			−1.0	−1.0	−1.0	−1.0
A_1	−1.2	−1.1	−1.0	−1.5	−1.5	−1.0
E	−3.5	−3.5	−0.8	−0.9	−1.1	−1.1
F_2^a	−2.8	−2.8	−1.8	−2.1	−1.8	−1.9
F_2^b	−2.5	−2.5	−0.7	−0.9	−0.7	−0.8
F_2^c			−0.6	−1.2		
F_2^d	−2.7	−2.8				
	−1.8	−1.7	−1.4	−1.6	−1.1	−1.2

the different modes of the same crystal can be interpreted as evidence that no resonance effects are dominant or that very weak ones are present; therefore, both $\Sigma_3(z)$ and $\Sigma_4(z)$ are independent of z.

The exception of the A_1 mode of Cu_3VS_4 is in fact due to anharmonic resonance effects, as will be discussed in Sec. VIII.

VII. DISCUSSION OF THE EXPERIMENTAL RESULTS

In this section the abnormal features encountered during our experiments are discussed.

A. Frequency of the A_1 mode

In Sec. V, it is mentioned that the frequency of the A_1 mode increases with the mass of the atom M. Zigone[13] also finds the same behavior with the impurity mode of ZnS:M (M is the transition metal) where the frequency increases with the mass of M. In a force-constant model, the frequency of this mode must be independent of the nature of atom M and, contrary to what happens here, this frequency decreases with M for numerous tetrahedral molecules of the form MX_4.[14] In the molecular case there is no lattice, so the interatomic distance is modified when the volume of M increases, keeping a roughly constant electronic overlap between M and X. If we take here a covalent picture to describe the bounding of the Cu_3MS_4 compounds, which is justified by the fact that the ionicity is very weak (see Sec. IV), we see that the M–S distance is fixed by the crystal lattice (see Table I) in such a way that the overlap between M and S increases as the atom M expands. The simplest assumption consists in taking a force constant proportional to the overlapping volume V and consequently a frequency ω varying as $V^{1/2}$. Figure 7 shows that the ω vs $V^{1/2}$ line is in fairly good agreement with the experimental points. This oversimplified model suggests that the frequency increase of the A_1 mode with M must be a size effect even if more detailed calculations are necessary to prove this.

B. A-peak doubling

An interesting result is the A_1-peak doubling for Cu_3NbS_4 and Cu_3TaS_4. In fact, in all kinds of experiments, a small satellite always preceded the normal A_1 peak for Cu_3NbS_4 and Cu_3TaS_4. Selection rules showed an A_1 character for this peak within the experimental accuracy of selection rules. In Table VIII, the frequencies, the FWHM, and relative intensities of the extraneous peaks labeled A' are reported. The FWHM of the A_1 peak of Cu_3VS_4 suggests the probable existence in that compound of such a satellite too close to the normal peak to be resolved by the experimental setup. But this hypothesis is questionable because there is a more plausible explanation for the abnormally high FWHM of that compound, as discussed in Sec. IIIC. Various assumptions can be made to explain this new peak.

It cannot be a double-phonon structure because its intensity relative to the A_1 peak remains constant with temperature.

A Jahn-Teller effect on the d electrons of the central atom would alter the overlap integrals between M and S. The normal-charge state of V is V^{5+} as shown from magnetic susceptibility measurements on Cu_3VS_4. Thus, no d electrons available for a Jahn-Teller distortion are present on V^{5+}. Thus the argument of a Jahn-Teller effect can be ruled out. The same kind of measurements performed on Cu_3TaS_4 have also shown the exis-

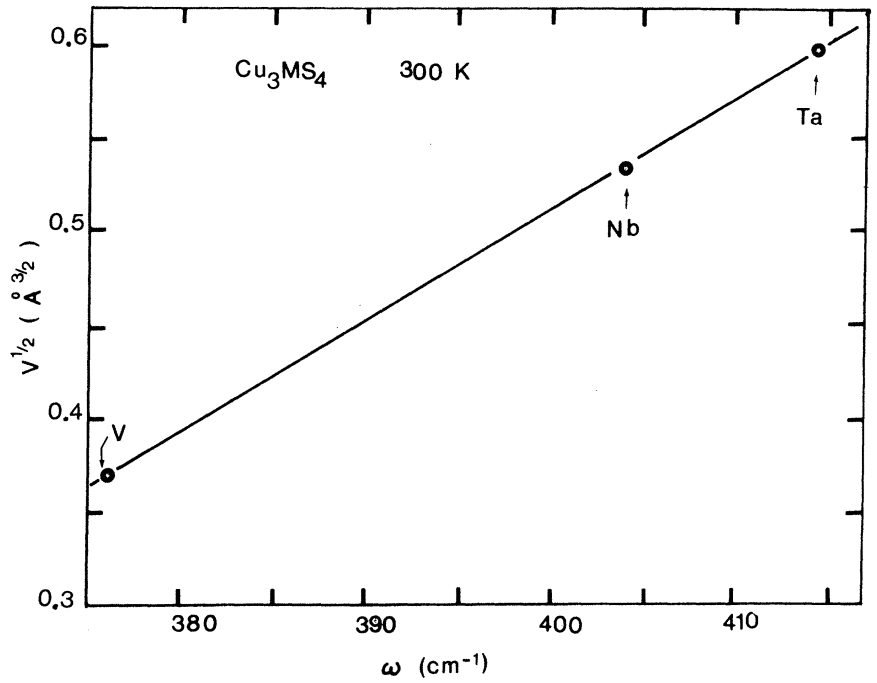

FIG. 7. Frequency of the A_1 mode versus overlap volume of M–S atoms.

tence of a diamagnetism only possible with a Ta^{5+} charge state.

A symmetry-lowering effect seems very unlikely. No unit-cell doubling is observed in x-ray experiments on Cu_3VS_4 and Cu_3TaS_4.

The hypothesis of an isotope effect is easily rejected, because the natural isotopes S^{32} (95%) and S^{34} (4.2%) would give for the satellite frequencies 363, 391, and 401.6 cm^{-1} instead of the observed ones, and would not explain the observed variations in the relative intensities.

The assumption of an inversion of a small number of copper and M atoms has been also roughly tested. A Cu atom in the place of an atom M implies different overlap integrals with the sulfur atoms giving satellite frequencies. However, preliminary x-ray experiments rejected such an inversion.

Therefore the peak doubling remains an open question with the experimental results available up to now.

TABLE VIII. Frequency ω and width 2Γ and relative intensity of the A-type modes for the Cu_3MS_4 compounds at 300 K.

Compound	ω	2Γ	$I_{A'}/I_{A_1}$
Cu_3VS_4	375.6	6.1	
Cu_3NbS_4	400.9	1.7	
	404	2	0.20
Cu_3TaS_4	403	2.5	
	414.3	3	0.01

C. High value of the FWHM of the Cu_3VS_4 A_1 mode

A simple inspection of Table IV reveals that 2Γ for the Cu_3VS_4 A_1 mode is, at all temperatures, between 77 and 300 K, 2 or 3 times higher than the corresponding values for Cu_3NbS_4 and Cu_3TaS_4. The hypothesis of a nonresolved satellite peak must be rejected. In fact, a Jahn-Teller distortion is not possible in view of the magnetic properties of Cu_3VS_4, and a population inversion of Cu and V would give a higher frequency for A' (near 400 cm^{-1} instead of 375 cm^{-1}).

The A_1 mode involves only the motion of sulfur atoms. X-ray experiments on Cu_3VS_4 (Ref. 3) showed a highly anharmonic motion for the sulfur with distortions in $\langle 11\bar{2}\rangle$ directions for that compound. Therefore, the situation can be visualized as the symmetric vibration of a quasirregular tetrahedron with nonfixed equilibrium positions at the corner for the atoms but changing along the $\langle 11\bar{2}\rangle$ directions. It is then evident that the M–S bond length changes continuously around a mean value, giving a rather large frequency distribution for the A_1 mode centered on 375.5 cm^{-1}.

D. Comparative study of the frequency and linewidth variations under pressure

The question that arises naturally is whether there exists any connection between the observed frequency changes and the changes in linewidth under pressure.

In our case we have followed the ω and Γ variations of the modes of all the compounds. Besides the A_1 mode of Cu_3VS_4, the variation of which is discussed in Sec. VIII, the frequency changes under pressure at a moderate rate of some cm^{-1} for 20 kbar. In contrast, Γ does not change within the experimental errors up to 20 kbar. As far as we know, this is the case for all experimental results reported in literature. Very often, pronounced variations of 100% in frequency are obtained, with changes in Γ, if any, less than 5%. Lowndes and Rastogi[15] have also reported pressure dependence of ω and Γ of alkali halides up to 6 kbar. Frequency variations are of the order of 20% but Γ does not change within the experimental error. Polian and Besson[16] also followed the modes of GaS up to 250 kbar without noticing a significant change in the linewidth of modes.

The physical reason for this behavior is the following. An externally applied hydrostatic pressure field is a static perturbation on the system Hamiltonian; its only effect is a continuous change of the eigenvalues (i.e., eigenfrequencies) of the system. Such a static perturbation cannot produce real transitions between the energy levels; an energy level being populated cannot be deexcited or further populated under this effect. So in a first approximation, hydrostatic pressure changes only the frequency of phonons, not affecting their lifetime because no real transitions are possible.[17]

Diagrammatically, this fact can be understood because the static pressure field can be considered as a zero-frequency phonon effect (i.e., the frequency spectrum of the static perturbation contains only a zero-frequency term).

But the lowest-order diagram that can effectively contain a zero-frequency phonon is

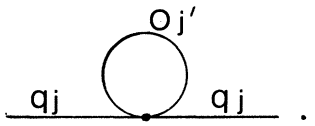

This diagram corresponds to a virtual process, and so it contributes only to the frequency shift, but not on the lifetime as it is expected by the previous argument.

Moreover, the coupling potential for such a diagram, $V(-\vec{q}j;\vec{q}j;\vec{q}'j';-\vec{q}'j')$, is independent of the frequency of the virtual phonon because in our case $q'=0$. Therefore $V(-\vec{q}j;\vec{q}j;\vec{q}'j';-\vec{q}'j')$ $\rightarrow V(-\vec{q}j;\vec{q}j)$, i.e., the above diagram shrinks to a point vertex

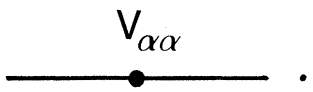

The self-energy contains now an insertion of point vertexes.

It is clear that the Grüneisen parameter is in a straightforward relation with these diagrams and in fact it is given[18] by the relation

$$\gamma(\vec{q},j)=-\frac{2}{3\hbar\omega(\vec{q},j)}\sum_{\alpha}V_{\alpha\alpha}(-\vec{q}j;\vec{q}j)\,,$$

where α spans the three directions of space. Diagrammatically, we can write

$B(\vec{q},j)=\sum_{\alpha}$ 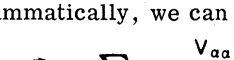 ,

where

$$B(\vec{q},j)=-\tfrac{3}{2}\gamma(\vec{q},j)\hbar\omega(\vec{q},j)$$

In conclusion, the frequency dependence on pressure is much more pronounced than that of the FWHM. This assertion is valid only in a case away from any anharmonic resonance. In the later case an abnormal behavior is obtained. Such an example is the FWHM of the A_1 mode of Cu_3VS_4, as is discussed in the next section.

VIII. ANHARMONIC RESONANCE OF THE LINEWIDTH OF THE A_1 MODE OF Cu_3VS_4

During pressure experiments on Cu_3VS_4 we observed a broadening of the A_1 peak near 20 kbar. Therefore, detailed experiments of the FWHM and the frequency of the A_1 mode as a function of pressure have been performed. Figures 8 and 9 give, respectively, the experimental results of the FWHM and frequency measurements. A resonantlike effect appears for the FWHM near 20 kbars. This effect is reversible and has been observed on four different samples. It is not related to a phase transition, although Cu_3NbS_4 and Cu_3TaS_4 exhibit such a phase transition in that region, because the other modes are affected neither in frequency nor in intensity within the experimental errors.

To explain the abnormal results, the lowest-order anharmonic diagram contributing to the FWHM is considered, i.e.,

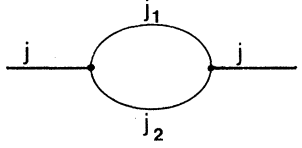

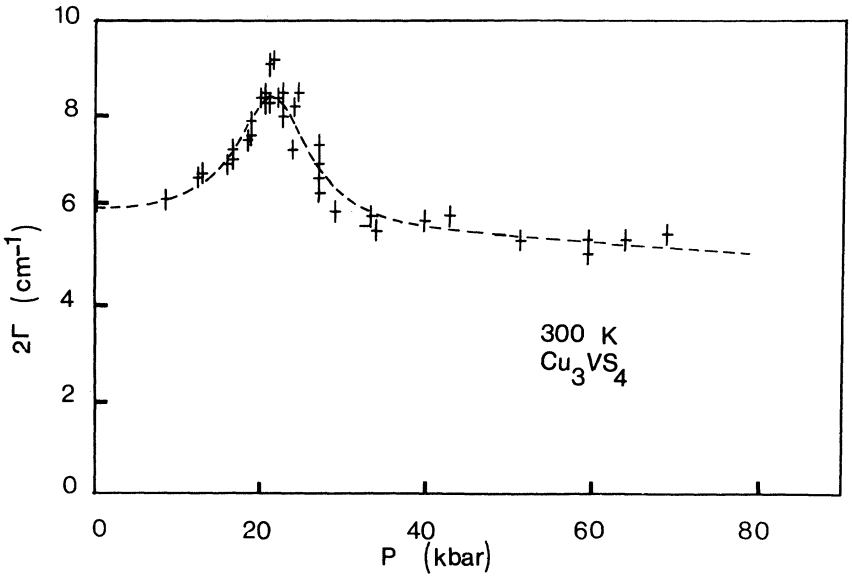

FIG. 8. Variation of the linewidth of the A_1 mode of Cu_3VS_4 as a function of the pressure. The full curve is fitted to experimental results as explained in the text.

The A_1 mode of Cu_3VS_4 varies very slowly as a function of pressure, keeping at practically a constant frequency in the pressure range 0–80 kbar. On the other hand, the two F_2 modes of lowest frequencies vary rapidly with pressure so that the relation

$$\omega_{A_1}(P) = \omega_{F_2^a}(P) + \omega_{F_2^b}(P) \tag{5}$$

is fulfilled near 20 kbar. The physical process described by the above diagram, according to which an A_1 phonon can excite two F_2 phonons and vice versa, is practically possible in the present case. As a matter of fact it is a symmetry-allowed process, since $F_2 \otimes F_2 = A_1 \oplus E \oplus F_1 \oplus F_2$, and the law of the conservation of energy is verified by virtue of Eq. (5).

Assuming that there exists a strong anharmonic interaction between the A_1 and the two F_2 modes and that the joint density of states for the two F_2 modes is singular inthe zone center, we obtain for the FWHM the following expression:

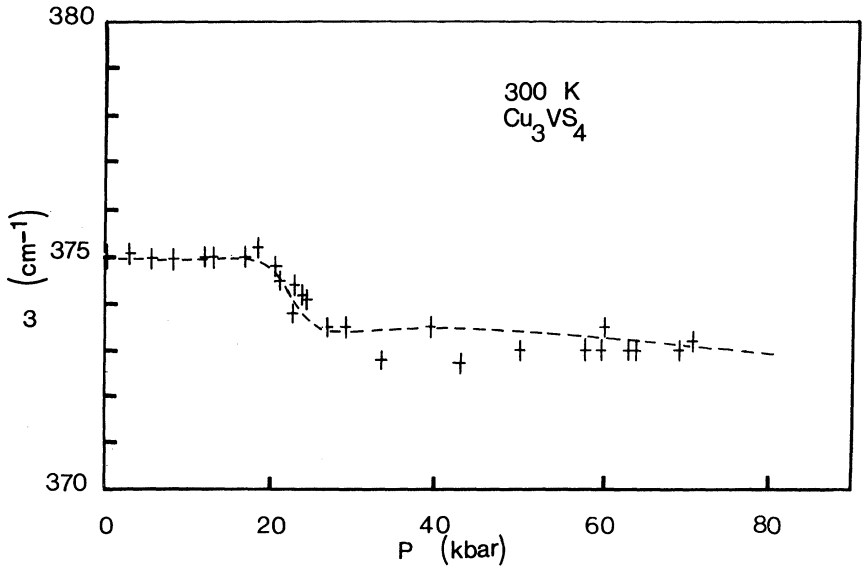

FIG. 9. Variation of the frequency of the A_1 mode of Cu_3VS_4 as a function of the pressure. The full curve is deduced by Kramers-Kronig analysis of that fitted on Fig. 8.

$$\Gamma = \frac{\Phi}{\omega_1 \omega_2}(n_1 + n_2 + 1)\frac{\gamma}{(\omega_{A_1} - \omega_1 - \omega_2)^2 + \gamma^2}, \quad (6)$$

where Φ is the interaction potential,

$$\omega_{1,2} = \omega_{1,2}(P) = \omega_0^{1,2} + \left(\frac{\partial \omega}{\partial P}\right)_{1,2} P, \quad (7)$$

and the population factors $n_{1,2}$ are only frequency dependent. So, expression (5) is only pressure dependent through $\omega_{1,2}$.

The quantity $\gamma/[(\omega_{A_1} - \omega_1 - \omega_2)^2 + \gamma^2]$ is an approximation for the joint density of states. Φ and γ are the adjusting parameters of the model. We tried to reproduce the resonant part of the FWHM curve superimposed on a constant FWHM background due to other anharmonic processes. The best fit with the experimental points is obtained for the values

$$\Phi \simeq 1.25 \times 10^5 \text{ cm}^{-4},$$

$$\gamma \simeq 5.5 \text{ cm}^{-1}.$$

Physically, γ represents the sum of half-widths at half-maximum (HWHM) for the two individual F_2 phonons. The fitted curve is shown in Fig. 8. On the other hand, the real part of the self-energy Δ is related to the imaginary part Γ by the Kramers-Kronig relation (for real processes as the one considered here), i.e.,

$$\Delta(\omega) = \frac{1}{\pi} \mathcal{P} \int_{-\infty}^{+\infty} \frac{\Gamma(\omega) d\Omega}{\Omega - \omega}$$

with the previously calculated parameters Φ and γ, Δ is computed as a function of pressure. Adding to the calculated value of Δ a slowly varying A_1 frequency of the form (in cm^{-1})

$$\omega_{A_1}(P) = 374.6 - 0.01P(\text{kbar})$$

(probably due to higher anharmonic contributions) we obtain the curve of Fig. 9, which reproduces the experimental data quite well.

The adopted model and the hypotheses made are consistent with other experimental results. The $F_2^a \otimes F_2^b$ double phonon decomposes as $A_1 \oplus E \oplus F_1 \oplus F_2$, which contains the infrared-active F_2 mode. Therefore an infrared-absorption experiment has been performed in the region between 300 and 400 cm^{-1}. Figure 10 shows the absorption coefficient due to the double-phonon structure. At a frequency corresponding approximately to the sum of F_2^a and F_2^b frequencies a strong absorption is observed which confirms the assumption of a strong joint density of states.

We tried to reproduce the absorption coefficient due to that double-phonon structure with the joint density of states determined by the fitting of Eq. (5) with an HWHM $\gamma = 5.5$ cm^{-1}. Figure 10 shows a fair agreement with the experimentally determined

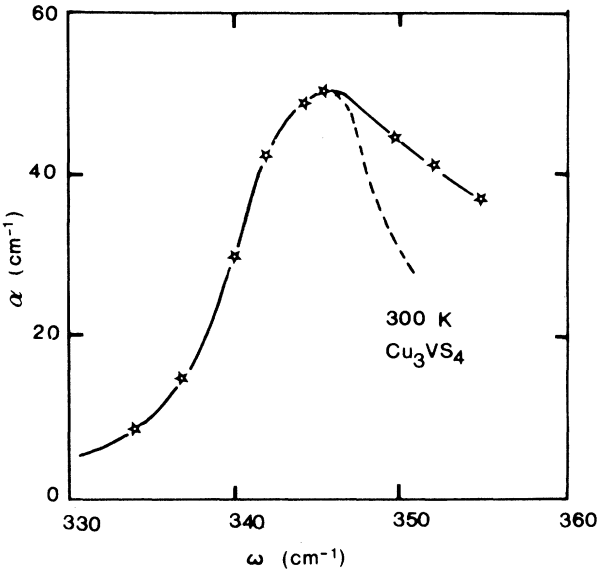

FIG. 10. Far-infrared absorption coefficient of Cu_3VS_4.

absorption coefficient.

The value obtained of ($\Phi = 1.25 \times 10^5$ cm^{-4}) for the anharmonic interaction must be considered as a strong coupling between the A_1 and the $F_2^a \oplus F_2^b$ phonons. In fact, Fig. 3 shows that the A_1 mode moves sulfur atoms along the cube diagonals and has nonzero projection on the F_2^b-mode motion. On the other hand, structural data[3] showed an abnormal anharmonic motion of the sulfur atoms as was previously explained. Therefore a strong coupling between modes involving the motion of sulfur atoms is expected through the sulfur atom anharmonicity. This assumption is supported by the following experimental fact: Near 60 kbar a crossing of the A_1 mode with the double phonon $2F_2^a$ occurs. No such an anharmonic resonance effect is obtained within experimental error. This is due probably to combined effects of a weak density of states for the $2F_2^a$ double phonon and a weak anharmonic coupling.

IX. CONCLUSION

In this paper, the study of the lattice vibrations of Cu_3MS_4 (M = V, Nb, Ta) are reported. All optically active modes have been detected, assigned, and most of them studied as a function of temperature and hydrostatic pressure.

Most of the modes have a "normal" behavior common to that found in the majority of semiconductors. The high anharmonicity of the Cu_3VS_4 modes (especially the E mode) could be connected with a possible disorder of copper ions.

An original effect of an anharmonic resonance is detected for the A_1 mode of Cu_3VS_4 and explained as an interaction of this mode with the combination of the F_2^a and F_2^b phonons.

The frequency of A_1 modes increases with M contrary to the molecular case. This fact is interpreted as an enhancement of the electronic overlap between M and S atoms due to the confinement of the MS_4 "molecule."

A satellite peak with an A symmetry not predicted by the group-theoretical analysis appears for $CuNbS_4$ and Cu_3TaS_4. Further experimental investigations are necessary to determine ambiguously the nature of that vibration.

[1]H. Arribart and B. Saporal, in *Proceedings of the Fourteenth International Conference on the Physics of Semiconductors, Edinburgh, 1978,* edited by B. L. H. Wilson (Institute of Physics, Bristol, 1978), p. 573.
[2]N. Le Nagard, Thèse d'Etat, Université Paris-Sud. Paris, 1975 (unpublished).
[3]F. J. Trojer, Am. Mineral 51, 890 (1966).
[4]N. Le Nagard and G. Collin, the results obtained by these authors are only partly published in Ref. 2; the remainder are unpublished.
[5]B. A. Weinstein and G. J. Piermarini, Phys. Rev. B 12, 1172 (1975).
[6]J. L. Warren and T. G. Worlton, Comput. Phys. Commun. 3, 88 (1972).
[7]R. Le Toullec. Thèse d'Etat, Université Pierre et Marie Curie, Paris, 1968 (unpublished).
[8]K. H. Schmidt, A. Müller, J. Bowner, and F. Jellinek, J. Mol. Structure 11, 275 (1972).
[9]A. A. Maradudin and A. G. Fein, Phys. Rev. 128, 2589 (1962).
[10]R. F. Wallis, I. P. Ipatova, and A. A. Maradudin, Fiz. Tverd. Tela (Leningrad) 8, 1064 (1966) [Sov. Phys.—Solid State 8, 850 (1966)].
[11]R. Zallen and M. L. Slade, Phys. Rev. B 18, 5775 (1978).
[12]D. Petritis, G. Martinez, and O. Gorochov, in *Proceedings of the Fourteenth International Conference on the Physics of Semoconductors, Edinburgh, 1978,* edited by B. L. H. Wilson (Institute of Physics, Bristol, 1978), p. 677.
[13]M. Zigone, K. Kung, P. Plumelle, and M. Vandevyver, in *Proceedings of the International Conference on Lattice Dynamics, Paris, 1977,* edited by M. Balkanski (Flammarion, Paris, 1978), p. 405.
[14]G. Herzberg, *Molecular Spectra and Molecular Structure* (Van Nostrand, Princeton, N.J., 1950).
[15]R. P. Lowndes and A. Rastogi, Phys. Rev. B 14, 3598 (1976).
[16]A. Polian, J. C. Chervin, and J. M. Besson, Phys. Rev. B 22, 3049 (1980).
[17]J. J. Sakurai, *Advanced Quantum Mechanics* (Addison-Wesley, Reading, Mass., 1967).
[18]R. A. Cowley, Rep. Prog. Phys. 31, 123 (1968).